NJC

PAPER

View Article Online
View Journal | View Issue

Cite this: *New J. Chem.*, 2018, **42**, 19062

Catalytic study on thermal decomposition of Cu-en/(AP, CL-20, RDX and HMX) composite microspheres prepared by spray drying

Nai-Meng Song,[a] Li Yang, *[a] Ji-Min Han,[a] Jian-Chao Liu,[a] Guo-Ying Zhang[a] and Hong-Xu Gao[b]

Received 15th August 2018,
Accepted 27th October 2018

DOI: 10.1039/c8nj04166k

rsc.li/njc

This paper mainly describes a spray drying method for the preparation of a variety of composite microspheres of energetic materials, including AP, RDX, β-HMX, and ε-CL-20, which are commonly used in composite modified double base propellants. The composite microspheres were prepared with catalyst Cu-en to increase the contact area between the energetic materials and the catalyst. The results of powder XRD and EDX suggest that copper is mainly distributed in the interior of AP and ε-CL-20 composite particles, but mainly dispersed on the surface of β-HMX and RDX microspheres. The data of the DSC test show that the catalytic effects of the composite microspheres exhibit the best performance, compared with the simply physically mixed catalyst and the energetic materials. The exothermic peak temperatures of AP, RDX, β-HMX, and ε-CL-20 are reduced to 305.4 °C, 228.6 °C, 280.2 °C and 232.0 °C, respectively. The results show that the composite microspheres can enlarge the contact area between the catalyst and the energetic materials thus enabling an enhanced catalytic effect.

Introduction

Ammonium perchlorate (AP) and nitramine explosives are important components of a composite modified double base (CMDB) propellant, and efforts to make new propellant complexes to improve the performance have been made in recent years. AP is one of the commonly used oxidants in composite solid propellants,[1] while hexanitrohexaazaisowurtzitane (CL-20), cyclotrimethylenetrinitramine (RDX) and 1,3,5,7-tetranitro-1,3,5,7-tetrazocane (HMX) have been used as energetic materials for the CMDB propellant ingredients.[2,3] The combustion behavior of the propellant is affected by the thermal decomposition pattern (AP, CL-20, RDX, and HMX).[4] In general, the thermal decomposition properties of AP, CL-20, RDX, and HMX can be improved through the addition of catalysts.[5,6] The catalytic efficiency of the catalyst depends on the contact area between the catalyst and the oxidant or energetic material,[7] as the increased contact area can accelerate a faster decomposition rate. At present, micro-nanoscale-sized catalysts are prepared to improve the catalytic efficiency by enlarging their specific surface area.[8,9] For example, nano-CuO can advance the decomposition peak temperature of AP and RDX.[5,7] Unfortunately, a nano-catalyst is vulnerable to aggregation, which affects its catalytic performance.[8,10] However, organometallic complex burning rate catalysts, such as copper organic chelates, have good dispersion properties and can enhance the burning rate significantly.[10] The organometallic complexes can generate the corresponding nanoscale metal oxide catalysts *in situ* during the combustion decomposition process.[11] Therefore, the research to optimize organometallic complex catalysts is a hot research topic.

Besides, the morphology and particle size of the catalyst have a great influence on its catalytic effect.[12] Among the fabrication methods developed thus far, spray drying is one of the most common methods for preparing micro spherical powders, essentially consisting of a one-step method for producing a powder product from raw materials typically in liquid forms, such as solution, suspension or paste.[13,14] (3,5-DNB)M M micro-nanospheres with a core–shell structure which could catalyze the thermal decomposition of AP were successfully produced by ultrasonic spray drying technology.[15] The spray drying technology can not only control the morphology of microspheroidal composite particles, but the powder prepared by spray drying also has good dispersion and no agglomeration.

$Cu(en)_2NO_3$ (ethylenediamine, en) is a stable copper-containing complex with a certain amount of nitrogen in the molecule and can be used as an energetic catalyst in CMDB propellants. The preparation of composite microspheres using catalysts and energetic materials can be a promising way to improve the thermal decomposition of propellants. This paper

[a] *State Key Laboratory of Explosion Science and Technology, Beijing Institute of Technology, Beijing 100081, P. R. China. E-mail: yanglibit@bit.edu.cn; Fax: +86-10-6891-1682; Tel: +86-10-6891-1682*
[b] *Xi'an Modern Chemistry Research Institute, Xi'an 710065, China*

aims to prepare composite microspheres of Cu-en and AP, CL-20, RDX or HMX by spray drying. XRD, SEM, EDS, and DSC are used to test the performance of the composite microspheres.

Experimental

Materials and methods

Ethylenediamine (analytical grade) was purchased from Tianjin Fuchen Chemical Reagent Factory. Ethyl acetate (analytical grade) and acetone (analytical grade) were purchased from Beijing Tong Guang Fine Chemicals Company. $Cu(NO_3)_2{\cdot}9H_2O$ (analytical grade) was supplied by Sinopharm Chemical Reagent Co, Ltd, Beijing, China. AP, RDX, β-HMX, and ε-CL-20 were provided by State Key Laboratory of Explosion Science and Technology (Beijing Institute of Technology). Surface morphology and microstructure were determined by scanning electron microscopy (SEM, S4800, Hitachi, Japan; operating at 15.0 kV). Thermal decomposition properties were measured by differential scanning calorimetry (DSC, CDR-4P, Shanghai Precision & Scientific Instrument Co., Ltd, China) at a heating rate of 10 °C min^{-1}. The powder diffraction of all samples was investigated by using a Bruker D8 Advance (Bruker, Germany) X-ray powder diffractometer (XRD) with a monochromatic diffracted beam using Cu-K_α radiation as the X-ray source operated at 40 kV and 40 mA.

Preparation of samples

The Cu-en solution was prepared and characterized according to the reported literature.[16] First, a solid powder of microspherical Cu-en was prepared by spray drying. The Cu-en powder and AP, RDX, ε-CL-20 or β-HMX are dissolved in the corresponding solvent in a certain mass ratio. The detailed information of the mixed solution is shown in Table 1.

L-217 (Beijing Laiheng Electronics Co., Ltd) is a type of commonly used spray drying equipment. The L-217 atomization method uses a two-fluid nozzle. The droplets produced by such nozzles have a particle size ranging from 10 μm to 1000 μm.[17,18] The product morphology and particle size can be controlled by adjusting the solution concentration, liquid intake, temperature, and cyclone wind speed. The wind speed of the cyclone is 36 m^3 h^{-1}, and the liquid inlet rate is controlled at 300 mL h^{-1}. The temperature in the preparation process is shown in Table 2.

In Table 2, T_i and T_o are inlet air temperature and outlet air temperature, respectively. The blower here refers to the amount of wind of the gas ring fan. PUMP is the inlet speed of the instrument. The temperature of the inlet air is set according to the boiling point of different solvents. Because of the danger of energetic materials, the maximum temperature is set at 110 °C to ensure the safety of the experiment.[19]

Table 1 Formulation of the mixed solutions

	AP/Cu-en	RDX/Cu-en	ε-CL-20/Cu-en	β-HMX/Cu-en
Ratio (g/g)	2 : 0.02	2 : 0.02	2 : 0.02	2 : 0.02
Solvent	Deionized water	Acetone	Ethyl acetate	Acetone
Volume (ml)	100	100	100	150
Class	Solution	Suspension	Suspension	Suspension

Table 2 The spray drying conditions

	T_i (°C)	T_o (°C)
Cu-en	110	84
AP/Cu-en (AP)	110	86
RDX/Cu-en (RDX)	80	62
β-HMX/Cu-en (β-HMX)	80	62
ε-CL-20/Cu-en (ε-CL-20)	90	70

Results and discussion

X-ray powder diffraction (XRD) test

In order to study the composition of these composite particles, the aggregation structures were determined by the XRD method. The XRD powder diffraction pattern was obtained in the range of $2\theta = 5^\circ$ to 60° to provide a clear view of each sample. The XRD data of individual components and composites are shown in Fig. 1.

Fig. 1(a) shows the comparison of data from the AP group. Obviously, all the characteristic peaks of AP are in good agreement with the peak of the complex. A careful comparison of the Cu-en and AP/Cu-en data shows that a characteristic peak of Cu-en emerges on the diffraction peak map of AP/Cu-en at $2\theta = 21.50^\circ$, but the two strongest peaks of Cu-en at 11.67° and 17.92° do not appear in the complex. Moreover, the characteristic peaks of Cu-en at $2\theta = 15.17^\circ$, 22.67°, and 30.87° can hardly appear since they overlap with the peaks of AP. This phenomenon suggests the good distribution of Cu-en in the particles, because the well soluble Cu-en can difficultly self-aggregate to form phase separation, resulting in a good dispersion among the AP complex. In conclusion, the results demonstrate that the packing mode of AP is not changed in this composite particle, while the Cu-en cannot generate phase separation.

The comparison of the diffraction peaks of the ε-CL-20 group is shown in Fig. 1(b). Undoubtedly, the peak of ε-CL-20 can be found in the corresponding position of ε-CL-20/Cu-en. Although the main peak of Cu-en was not clearly revealed in ε-CL-20/Cu-en, after careful observation of the diffraction peak of ε-CL-20/Cu-en, weak protrusions are found at $2\theta = 11.54^\circ$, 15.01°, 17.80°, and 31.11°. These weak protrusions are at the same angle as the characteristic peak of Cu-en. It can be confirmed that this change is caused by doping with Cu-en. Since the peak position of Cu-en is similar to that of ε-CL-20, and the proportion of ε-CL-20 is much higher than that of Cu-en, the peak of Cu-en is not obvious in the composite. There is a small peak at $2\theta = 22.48^\circ$ in ε-CL-20/Cu-en, which corresponds to the peak of $2\theta = 22.67^\circ$ in Cu-en. Combining this evidence comprehensively, we can conclude that Cu-en exists as a larger domain in this complex.

Fig. 1(c) shows the results of the RDX group. Comparing the data of RDX and RDX/Cu-en, it can be found that diffraction peaks of RDX can be clearly found in the diffraction peaks of RDX/Cu-en. The diffraction peaks corresponding to Cu-en appear in the diffraction pattern of RDX/Cu-en when $2\theta = 11.52^\circ$

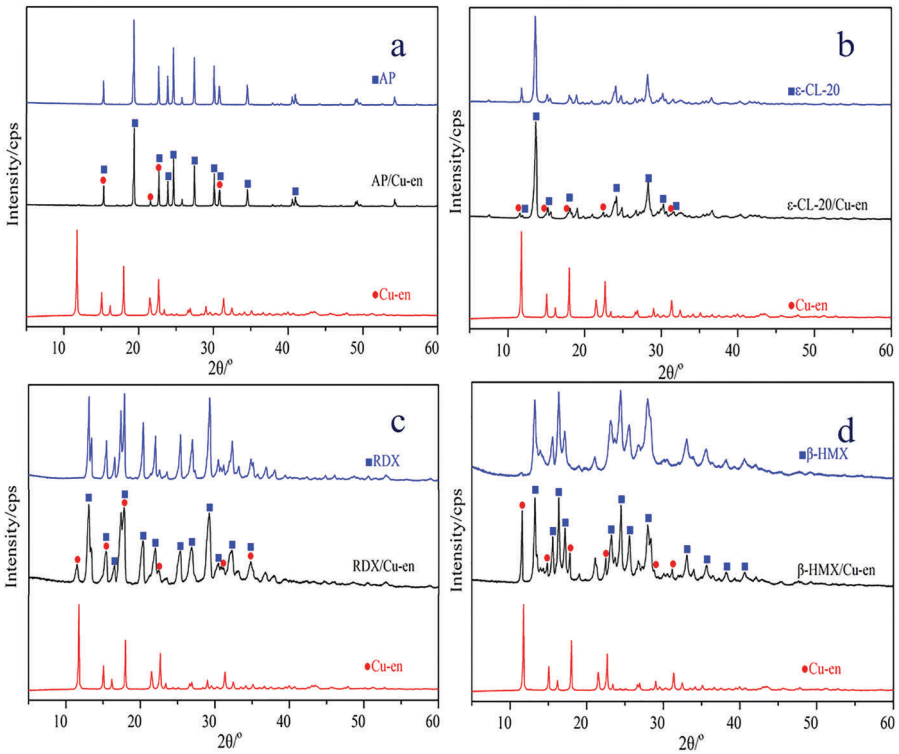

Fig. 1 XRD patterns of product samples: (a) AP group, (b) ε-CL-20 group, (c) RDX group and (d) β-HMX group.

and 22.49°. The other obvious characteristic peak of Cu-en overlaps with RDX and appears together at 2θ = 17.81°. The three main characteristic peaks of Cu-en can be found in the graph of RDX/Cu-en. Similarly, the results of the β-HMX group data in Fig. 1(d) also illustrate that the peaks of β-HMX/Cu-en are the superposition of the peaks of β-HMX and Cu-en. As a result, both RDX/Cu-en and β-HMX/Cu-en are a mixture of Cu-en and energetic materials.

In summary, from the results of XRD, the peaks of Cu-en in RDX/Cu-en and β-HMX/Cu-en are more obvious. The diffraction peak of Cu-en is relatively weak in ε-CL-20/Cu-en. There is a small amount of Cu-en peak in the diffraction peak of AP/Cu-en, and most of the peaks in these peaks are overlapping peaks of Cu-en and AP.

The plausible reason is due to the varied solubility of Cu-en in different solvents. Since the solubility of Cu-en in water is greater than that of AP, the AP first reaches saturation and precipitates during evaporation of the droplets. As the solvent in the droplet surface volatilizes, most of the Cu-en rapidly moves towards the center of the droplet. When the evaporation process is complete, most of the Cu-en is distributed inside the particles, and only a small part of the Cu-en is present on the surface of the particles. As the Cu-en did not form larger domains and highly ordered aggregation, the XRD only collected a few characteristic peaks of Cu-en. Such dispersion is believed to be an efficient way to increase the contact area. In the meantime, Cu-en is only slightly soluble in ethyl acetate, so that Cu-en may start to crystallize along with ε-CL-20, resulting in the weak diffraction peaks of Cu-en in the composite. In contrast, the Cu-en is insoluble in acetone. During evaporation of the droplets, insoluble Cu-en precipitates before the energetic materials. Therefore, the strong characteristic peaks of Cu-en can be clearly detected in RDX/Cu-en and β-HMX/Cu-en, but the phase separation is not conducive for enlarging the contact area between the catalyst and materials.

Energy dispersive spectrometer (EDS) analysis was used to scan the distribution of elements in a certain area to study the distribution of copper. The right column in Fig. 2 shows the distribution of copper in the composite particles. The green dots in the figure represent copper elements. Although the peaks of Cu-en are weak in the XRD peaks of the complex of AP/Cu-en and ε-CL-20/Cu-en, the results of EDS show that the copper element is present in the particle. The strong Cu signals prove that the AP or ε-CL-20 forms a composite particle doped with Cu-en.

Elemental analysis and morphological characteristics

From the comparison of SEM images, it can be seen that the morphology and particle size of the composite particles do not change after being doped with a small amount of Cu-en compared with the pure materials (AP, ε-CL-20, β-HMX, and RDX). Compared to the morphology of AP (or AP/Cu-en), the particles of ε-CL-20 (or ε-CL-20/Cu-en), β-HMX (or β-HMX/Cu-en) and RDX (or RDX/Cu-en) are regular spheres. Although the particle shape of AP is not regular, there are still a few particles that tend to be spherical in shape. In addition to the instrumental conditions, the size of the droplets is also related to the surface tension, density, and viscosity of the solution.[18,20] The relationship between

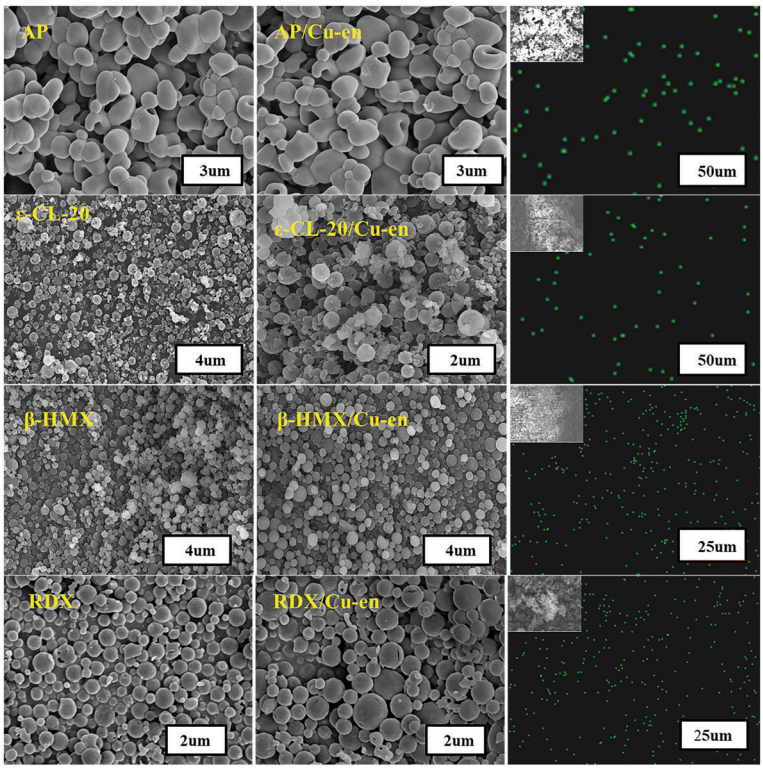

Fig. 2 SEM images of the particles and the distribution of Cu elements in composite microspheres.

the droplet size and the natural properties of the solution is as follows:

$$D_d = K_f \cdot Q^n [\rho^a \cdot \sigma^b \cdot \mu^c] \quad (1)$$

where K_f, Q, and n are the instrument constants (*i.e.*, frequency, pressure, and carrier gas velocity; which depend on the type of atomizer), the volumetric flow rate, and the power constant of volumetric flow rate, respectively. The symbols a, b, and c are the power constants of precursor properties: the density, the surface tension, and the viscosity, respectively.[21]

In this work, the solvents to prepare the precursor solutions of the AP and ε-CL-20 are water and ethyl acetate, respectively. While the precursor solutions of other samples were prepared by using acetone as the solvent. The surface tension and the viscosity of ethyl acetate (23.75 mN m^{-1}, 0.426 mPa s, 25 °C) and acetone (23.7 mN m^{-1}, 0.316 mPa s, 25 °C) are obviously smaller than those of water (72.14 mN m^{-1}, 0.8903 mN S m^{-2}, 25 °C).

It can be seen from eqn (1) that the size of the droplets formed by the atomization of the AP solution is larger than the droplets formed by the atomization of the other three solutions. The SEM images demonstrate that the particle size distribution of AP (or AP/Cu-en) is in the range of 2–4 μm. The size of ε-CL-20 (or ε-CL-20/Cu-en), β-HMX (or β-HMX/Cu-en), and RDX (or RDX/Cu-en) particles is as small as 1 μm to 2 μm.

In general, the conversion of droplets into solid particles is instantaneously accomplished during the spray drying process. However, when the droplet size is too large, the drying efficiency also decreases, causing the liquid–solid phase transition time to be prolonged. The longer the liquid–solid phase transition time, the more affected the morphology of the particles by the gas flow. Therefore, the shape of the droplets of the AP (or AP/Cu-en) was deformed due to the influence of the gas flow during the process of liquid–solid phase transition. Finally, the shape of the AP after spray drying is not a regular sphere. Since the natural properties of acetone and ethyl acetate are superior to those of water, the droplets formed by suspension of ε-CL-20 (or ε-CL-20/Cu-en)/β-HMX (or β-HMX/Cu-en)/RDX (or RDX/Cu-en) complete the liquid–solid phase transition just after being sprayed into the drying tower. The effect of gas flow on the morphology of the particles is avoided. The state change of the droplet during the spray drying process is shown in Fig. 3.

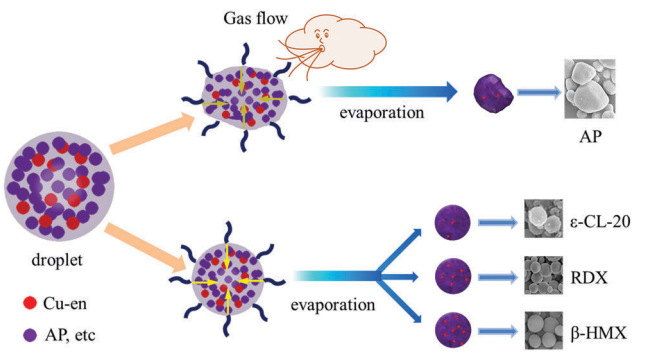

Fig. 3 The mechanism for preparing composite particles by the spray drying method.

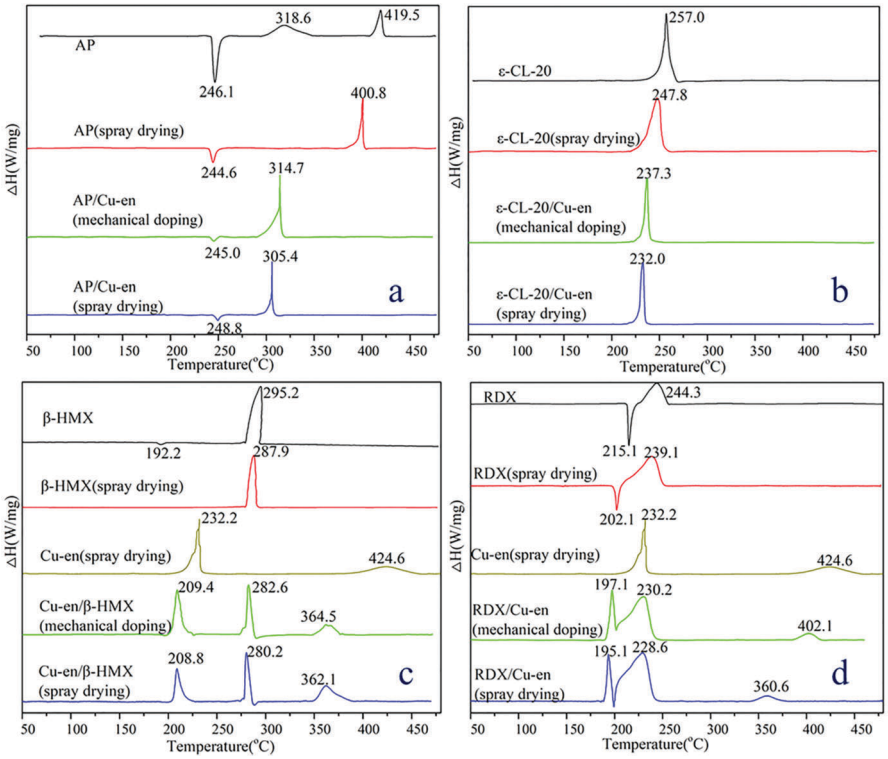

Fig. 4 DSC curves of the (a) AP group, (b) ε-CL-20 group, (c) β-HMX group and (d) RDX group.

The catalysis effect of Cu-en on the decomposition of AP/CL-20/β-HMX/RDX

Fig. 4(a) shows DSC curves of the AP group. The DSC curve of raw AP shows one endothermic peak and two exothermic peaks. The DSC curves show an endothermic peak at 246.1 °C, which is attributed to the crystal transformation of AP from orthorhombic form to cubic phase. The thermal decomposition of AP occurs in two steps. The first exothermic peak with the peak temperature 318.6 °C (low-temperature decomposition, LTD) corresponds to the partial decomposition of AP and formation of an intermediate product. The second, main exothermic peak with the peak temperature 419.5 °C (high-temperature decomposition, HTD) corresponds to the complete decomposition of the intermediate product into volatile products.[22,23]

The process of thermal decomposition of micro AP which was prepared by spray drying has been simplified into two steps. The first endothermic peak concerning the crystal transformation was at a temperature of 244.6 °C, which was essentially unchanged from the raw AP. However, it can be clearly seen that the peak shape of the endothermic peak becomes small. This is because the particle size of the micro AP is small and the morphology is regular, so the energy required for the process of crystal transformation is reduced. For microsphere AP, there is one peak at 400.8 °C corresponding to the HTD step as shown in its DSC curves. This slight decrease is because the internal stress formed by decomposition products is not intensive enough to crack the AP crystal into smaller grains. Therefore, there is no significant LTD step because the NH_3 formed in the initial steps overspreads the crystal surface of micro AP.[24]

The catalytic effect of Cu-en on AP was studied by comparing two different mixing methods. By mechanically mixing micro spherical Cu-en with micro AP, it can be found that the peak of HTD decreases from 400.8 °C to 314.7 °C. The temperature of the HTD peak of the micro AP/Cu-en prepared by the spray drying method is 305.4 °C, which is 95.4 °C earlier than the micro AP. Obviously, it can be seen that the way of preparing composite particles has a better catalytic effect.

The mechanical doping method only allows the particles of Cu-en to contact with the surface of AP particles, and the catalyst in the composite particles is distributed throughout the particles to make it have a wider contact area with the AP. In summary, the greater the contact area between the Cu-en and AP, the more catalytic sites there are and the better catalytic effect.

In the view of the electron-transfer mechanism,[25,26] the presence of partially filled Cu^{2+} 3d orbitals may accelerate the process of electron-transfer:

$$NH_4ClO_4 \rightarrow NH_4^+ + ClO^- \quad (2)$$

$$Cu^{2+} + ClO^- \rightarrow Cu^+ + ClO_4^\bullet \quad (3)$$

$$Cu^+ + NH_4^+ \rightarrow Cu^{2+} + NH_4^\bullet \quad (4)$$

From step (3) and (4), it can be seen that Cu^{2+} acts as an intermediate transfer. A positive hole in Cu^{2+} can accept

Table 3 The decomposition heat of AP and nitramine explosives

ΔH (J g^{-1})	AP	AP(spray drying)	AP/Cu-en(mechanical doping)	AP/Cu-en(spray drying)
	294.2	446.8	784.6	840.4
ΔH (J g^{-1})	ε-CL-20	ε-CL-20(spray drying)	ε-CL-20/Cu-en(mechanical doping)	ε-CL-20/Cu-en(spray drying)
	1886.4	2049.2	2240.3	2322.4
ΔH (J g^{-1})	β-HMX	β-HMX(spray drying)	β-HMX/Cu-en(mechanical doping)	β-HMX/Cu-en (spray drying)
	1566.8	1742.5	1906.2	1944.8
ΔH (J g^{-1})	RDX	RDX(spray drying)	RDX/Cu-en(mechanical doping)	RDX/Cu-en(spray drying)
	840.8	1142.4	1286.2	1311.5

electrons from perchlorate ions enhancing step (2). Currently, this catalytic mechanism is not yet fully understood.

DSC data show that compared with the decomposition peak temperature of raw ε-CL-20, the micro-spherical ε-CL-20 lowers the temperature from 257.0 °C to 247.8 °C (in Fig. 4(b)). The decomposition peak of the mixed micro spherical ε-CL-20/Cu-en (mechanical doping) is reduced to 237.3 °C. The temperature of the decomposition peak of the micro ε-CL-20/Cu-en prepared by the spray drying method is 232.0 °C. Compared with the micro-spherical ε-CL-20, the two mixing methods reduced the decomposition peak temperature by 10.5 °C and 15.8 °C, respectively. As with the previous description of the AP group, the composite microspheres produced by spray drying have more satisfactory effects.

The DSC curve of the β-HMX group is shown in Fig. 4(c). Similar to the weakening of the crystal transformation peak of the AP, the crystal transition peak of the micro-spherical HMX at 192.2 °C was not found. The decomposition peak of micro-spherical β-HMX is reduced by 7.3 °C compared to the raw material. Compared with the decomposition peak temperature of micro-spherical β-HMX, the mechanical doping lowers the required temperature by 5.3 °C, and spray mixing lowers it by 7.7 °C. In Fig. 4(d), the endothermic peak at 215.1 °C is due to the melting of raw RDX. The exothermic peak at 244.3 °C is attributed to the decomposition of RDX to form a product such as CO, N_2, N_2O, NO_2, *etc.*[27] After the raw material RDX was prepared into micro spherical RDX, the exothermic peak temperature decreased by 5.2 °C. The exothermic peak temperature of RDX/Cu-en is 230.2 °C, which is 8.9 °C earlier than that of micro-spherical RDX. During the thermal decomposition of micro-spherical RDX/Cu-en composite, this reduction reached 10.5 °C. Regardless of the manner in which Cu-en is mixed with β-HMX or RDX, it can be seen that the peak of Cu-en occurs during the decomposition of the mixture. Cu-en has a strong exothermic peak at 232.2 °C and a weak exothermic peak at 424.6 °C. Due to mixing with β-HMX or RDX, the temperature of the two exothermic peaks of Cu-en has significantly advanced. In contrast, the Cu-en can accelerate the thermal decomposition of the β-HMX (or RDX), and the β-HMX (or RDX) can also change the thermal decomposition process of the Cu-en.[28]

ε-CL-20, β-HMX, and RDX are typical nitramine explosives. There are a large number of C–N and N–N bonds present in their molecules.[29,30] The outer layer electron of Cu exhibits s–d hybrid orbitals, making it slightly conductive with weak chemical activity. This would weaken the C–N and N–N bond strengths, promoting the unimolecular decomposition of nitramine explosives.[31]

The DSC data of the four composite microspheres compared with the data after mechanical doping with catalyst Cu-en, the exothermic peak temperatures of AP, ε-CL-20, β-HMX, and RDX were advanced by 9.3 °C, 5.3 °C, 2.4 °C and 1.6 °C, respectively. Thus, this kind of composite microsphere has a good application prospect in the CMDB propellant, especially in the propellant with AP and ε-CL-20 as the main components.

The decomposition heat of AP and its mixtures with Cu-en is determined by integration of the exothermic peak areas, and detailed data are shown in Table 3. The decomposition heat of AP(spray drying), AP/Cu-en(mechanical doping) and AP/Cu-en(spray drying) increases from 294.2 J g^{-1} to 446.8 J g^{-1}, 784.6 J g^{-1} and 840.4 J g^{-1}, respectively. Observing the data of group ε-CL-20, β-HMX and RDX, one can also find the same pattern. The data prove that the micro-spherical composite shows the best catalytic effect.

Conclusions

In this experiment, a variety of microspheres were prepared by spray drying. The results of XRD and SEM show that catalyst Cu-en and AP formed composite particles with sizes in the range from 2 μm to 4 μm. Cu-en and ε-CL-20, β-HMX or RDX formed regular shaped composite microspheres with a diameter of 1–2 μm. This micro-spherical composite particle exhibited excellent properties. Thermal analysis data of AP showed that when the particle size was reduced to a few microns, the LTD and HTD of its raw material were reduced to an exothermic peak at 400.8 °C. The composite particles prepared by spray drying have the best catalytic effect and can reduce the decomposition temperature of AP by 95.4 °C. Compared with the raw ε-CL-20, β-HMX and RDX, the peak temperature of their exothermic peaks were reduced to different extents after spheroidization. However, the peak temperature had a greater reduction after added Cu-en. The lowest exothermic peak temperatures for ε-CL-20, β-HMX and RDX are 232 °C, 280.2 °C, and 228.6 °C, respectively. All in all, the micro-spherical composite particles prepared by spray drying have an excellent catalytic effect on AP and nitramine explosive components in the CMDB propellant.

Conflicts of interest

There are no conflicts to declare.

Acknowledgements

We gratefully acknowledge financial support from the National Natural Science Foundation of China (No. 11672040), the State Key Laboratory of Explosion Science and Technology (No. YB2016-17) and the Beijing Institute of Technology Research Fund Program for Young Scholars. We thank the reviewers for their most valuable comments.

References

1 C. Oommen and S. R. Jain, Ammonium nitrate: a promising rocket propellant oxidizer, *J. Hazard. Mater.*, 1999, **67**(3), 253–281.
2 R. Yang, H. An and H. Tan, Combustion and thermal decomposition of HNIW and HTPB/HNIW propellants with additives, *Combust. Flame*, 2003, **135**(4), 463–473.
3 S. H. Kim, B. W. Nyande and H. S. Kim, *et al.*, Numerical analysis of thermal decomposition for RDX, TNT, and Composition B, *J. Hazard. Mater.*, 2016, **308**, 120–130.
4 D. V. Survase, M. Gupta and S. N. Asthana, The effect of Nd_2O_3, on thermal and ballistic properties of ammonium perchlorate (AP) based composite propellants, *Prog. Cryst. Growth Charact. Mater.*, 2002, **45**(1–2), 161–165.
5 L. Chen, L. Li and G. Li, Synthesis of CuO nanorods and their catalytic activity in the thermal decomposition of ammonium perchlorate, *J. Alloys Compd.*, 2008, **464**(1), 532–536.
6 R. Dubey, P. Srivastava and I. P. S. Kapoor, *et al.*, Synthesis, characterization and catalytic behavior of Cu nanoparticles on the thermal decomposition of AP, HMX, NTO and composite solid propellants, part 83, *Thermochim. Acta*, 2012, **549**(23), 102–109.
7 H. Ren, Y. Y. Liu and Q. J. Jiao, *et al.*, Preparation of nanocomposite PbO CuO/CNTs via microemulsion process and its catalysis on thermal decomposition of RDX, *J. Phys. Chem. Solids*, 2010, **71**(2), 149–152.
8 Q. L. Yan, F. Q. Zhao and K. K. Kuo, *et al.*, Catalytic effects of nano additives on decomposition and combustion of RDX-, HMX-, and AP-based energetic compositions, *Prog. Energy Combust. Sci.*, 2016, **57**, 75–136.
9 A. M. Kawamoto, L. C. Pardini and L. C. Rezende, Synthesis of copper chromite catalyst, *Aerosp. Sci. Technol.*, 2004, **8**(7), 591–598.
10 J. Gao, L. Wang and H. Yu, *et al.*, Recent Research Progress in Burning Rate Catalysts, *Propellants, Explos., Pyrotech.*, 2011, **36**(5), 404–409.
11 T. T. Nguyen, *The effects of ferrocenic and carborane derivative burn rate catalysts in AP composite propellant combustion: mechanism of ferrocene-catalysed combustion*, DSTO Aeronautical and Maritime Research Laboratory, 1995, pp. 1–39.
12 A. B. D. Nandiyanto and K. Okuyama, Progress in developing spray-drying methods for the production of controlled morphology particles: From the nanometer to submicrometer size ranges, *Adv. Powder Technol.*, 2011, **22**(1), 1–19.
13 B. R. Bhandari and T. Howes, Implication of glass transition for the drying and stability of dried foods, *J. Food Eng.*, 1999, **40**(1-2), 71–79.
14 D. Das and T. A. G. Langrish, Combined Crystallization and Drying in a Pilot-Scale Spray Dryer, *Drying Technol.*, 2012, **30**(9), 998–1007.
15 W. Zhao, T. Zhang and N. Song, *et al.*, Assembly of composites into a core–shell structure using ultrasonic spray drying and catalytic application in the thermal decomposition of ammonium perchlorate, *RSC Adv.*, 2016, **6**(75), 71223–71231.
16 J. L. Burba, The Orientation and Interaction of Ethylenediamine Copper(II) with Montmorillonite, *Clays Clay Miner.*, 1977, **25**(2), 3059–3072.
17 F. Iskandar, Nanoparticle processing for optical applications – a review, *Adv. Powder Technol.*, 2009, **20**(4), 283–292.
18 A. B. D. Nandiyanto and K. Okuyama, Progress in developing spray-drying methods for the production of controlled morphology particles: From the nanometer to submicrometer size ranges, *Adv. Powder Technol.*, 2011, **22**(1), 1–19.
19 F. Nie, Z. Ma and B. Gao, *et al.*, Facile, continuous and large-scale production of core-shell HMX@TATB composites with superior mechanical properties by a spray-drying process, *RSC Adv.*, 2015, **5**(27), 21042–21049.
20 W.-N. Wang, A. Purwanto, I. W. Lenggoro, K. Okuyama, H. Chang and H. D. Jang, Investigation on the Correlations between Droplet and Particle Size Distribution in Ultrasonic Spray Pyrolysis, *Ind. Eng. Chem. Res.*, 2008, **47**, 1650–1659.
21 W. Y. Zhao, T. L. Zhang and L. N. Zhang, *et al.*, Large-scale production of (2,4-DHB) nM micro-nano spheres by spray drying and their application as catalysts for ammonium perchlorate, *J. Ind. Eng. Chem.*, 2016, **38**, 73–81.
22 Z. Zhou, S. Tian and D. Zeng, *et al.*, MOX (M = Zn, Co, Fe)/AP shell–core nanocomposites for self-catalytical decomposition of ammonium perchlorate, *J. Alloys Compd.*, 2012, **513**(2), 213–219.
23 L. Liu, F. Li and L. Tan, *et al.*, Effects of Nanometer Ni, Cu, Al and NiCu Powders on the Thermal Decomposition of Ammonium Perchlorate, *Propellants, Explos., Pyrotech.*, 2004, **29**(1), 34–38.
24 J. Zhi, W. Tian-Fang and L. Shu-Fen, *et al.*, Thermal behavior of ammonium perchlorate and metal powders of different grades, *J. Therm. Anal. Calorim.*, 2006, **85**(2), 315–320.
25 L. L. Bircumshaw and B. H. Newman, The Thermal Decomposition of Ammonium Perchlorate. II. The Kinetics of the Decomposition, the Effect of Particle Size, and Discussion of Results, *Proc. R. Soc. A*, 1955, **227**(1169), 228–241.
26 Y. Wang, X. Xia and J. Zhu, *et al.*, Catalytic Activity of Nanometer-Sized CuO/FeO on Thermal Decomposition of AP and Combustion of AP-Based Propellant, *Combust. Sci. Technol.*, 2010, **183**(2), 154–162.
27 X. Q. Shi, X. H. Jiang and L. D. Lu, *et al.*, Structure and catalytic activity of nanodiamond/Cu nanocomposites, *Mater. Lett.*, 2008, **62**(8–9), 1238–1241.
28 S. Mathew, K. Krishnan and K. N. A. Ninan, DSC Study on the Effect of RDX and HMX on the Thermal Decomposition

of Phase Stabilized Ammonium Nitrate, *Propellants, Explos., Pyrotech.*, 1998, **23**(3), 150–154.

29 V. K. Balakrishnan, A. Halasz and J. Hawari, Alkaline hydrolysis of the cyclic nitramine explosives RDX, HMX, and CL-20: new insights into degradation pathways obtained by the observation of novel intermediates, *Environ. Sci. Technol.*, 2003, **37**(9), 1838–1843.

30 J. C. Sanchez and W. C. Trogler, Efficient blue-emitting silafluorene–fluorene-conjugated copolymers: selective turn-off/turn-on detection of explosivesm, *J. Mater. Chem.*, 2008, **18**(26), 3143–3156.

31 U. R. Nair, R. Sivabalan and G. M. Gore, *et al.*, Hexanitrohexa-azaisowurtzitane (CL-20) and CL-20-based formulations (review), *Combust., Explos. Shock Waves*, 2005, **41**(2), 121–132.